A Three Parameter Underwater Image Formation Model

Henryk Blasinski, Stanford University, Stanford, CA, Joyce Farrell, Stanford University, Stanford CA

Abstract

We developed an underwater image formation model that describes how light is absorbed and scattered by seawater and its constituents. We use the model to predict digital camera images of a reference target with known spectral reflectance at different distances and depths. We describe an inverse estimation method to derive three model parameters: phytoplankton absorption spectrum, chlorophyll concentration and the amount of color dissolved organic matter or CDOM. The estimated parameters predict the spectral attenuation of light which can be used to color balance the images. In addition parameter estimates can be used to monitor environmental changes turning a consumer digital camera into a scientific measurement device.

Introduction

The digital camera has become an accessory that most people take with them everywhere, including underwater. Sadly, they are often disappointed with the quality of their underwater images. Backscattered light reduces image contrast and wavelength dependent light absorption by water introduces color changes [3, 20]. No doubt the quality of underwater photography will improve as the low-light sensitivity of imaging sensors increases and as new image processing methods are introduced.

Several underwater image correction algorithms operating on RGB images have been proposed [9, 19], but only a few methods analyze the data in the spectral domain [1, 2, 4]. In most cases, the goal of these algorithms is to improve and color rendering, rather than infer biologically relevant quantities [4, 14, 25]. In this paper we consider how to derive scientific data from underwater camera sensor images in order to characterize the ocean seawater environment. We also illustrate how this data can be used to process and improve the perceived quality of underwater images.

We developed an underwater image formation model to describe how light is absorbed and scattered by water and its constituents and how light is captured by the imaging sensor in a digital camera. We use our model to simulate the appearance of images captured by digital cameras and to relate the appearance to physically interpretable quantities, such as the type and amount of phytoplankton and other organic and inorganic matter in sea water [16]. We also use the insights we gained from these simulations to improve the way we process underwater images in order to produce more aesthetically pleasing photographs [4].

Our underwater image formation model is composed of three components. First, we use the underwater image formation model of Jaffe and McGlamery [13, 15] to describe light absorption and scattering in units of medium beam absorption and scattering coefficients. Second, we incorporate the results of oceanographic and biological research describing attenuation and scattering coefficients as functions of concentrations of fundamental constituents of sea water: phytoplankton, color dissolved organic matter (CDOM) and non-algal particles (NAP) [16]. Third, we use a full camera simulation package (ISET, [10]) to produce simulated images of underwater targets.

We use the underwater image formation model to predict the sensor data captured by a digital camera at a fixed distance and depth from a reference target with known spectral reflectance. With the appropriate parameter settings, we can reproduce the appearance of sensor images captured by real cameras in similar underwater environments.

We wish to use the digital camera as a scientific instrument that can measure environmental factors, such as the type and concentration of phytoplankton and other material in the seawater. To accomplish this, we introduce an inverse estimation method that uses the camera sensor data to derive parameters that describe 1) the spectral absorption of light by phytoplankton, 2) the concentration of chlorophyll in phytoplankton, and 3) the amount of color dissolved organic matter or CDOM.

We use the inverse estimation method as a metric to evaluate how well any digital camera can be used to measure environmental parameters and consider how these measurements can also be used to improve the perceived quality of underwater images.

Image formation model

The measurement m produced by an imaging device is linearly related to device's spectral sensitivity functions $p(\lambda)$ and the light radiance $\rho(\lambda)$ reaching the photodetector [24]

$$m = \int p(\lambda)\rho(\lambda)d\lambda. \tag{1}$$

A ray of light traveling between the source and the scene interacts with the medium in two ways. First, some of the light may be absorbed by the medium, and thus the overall intensity of light is reduced. Second, the direction of propagation of a portion of the light ray may be changed in a phenomenon called scattering. As a consequence these interactions the total radiance along a particular ray of light $\rho(\lambda)$ reaching an imaging device can be decomposed into two additive components; direct $\rho_d(\lambda)$ and backscattered $\rho_b(\lambda)$ [3, 13, 15]

$$\rho(\lambda) = \rho_d(\lambda) + \rho_b(\lambda). \tag{2}$$

The direct component contains all the light rays that, having been emitted by a source, interact with a scene. The backscattered component represents all the light rays whose direction of propagation was changed by the medium before they reached the target, which means they are captured by the imaging device without interacting with the scene (Fig. 1).

The McGlamery-Jaffe underwater image formation model [13, 15] describes how the absorption and scattering affect the direct and backscattered radiance components. However, for uniform surfaces at a fixed distance from the camera the radiance of

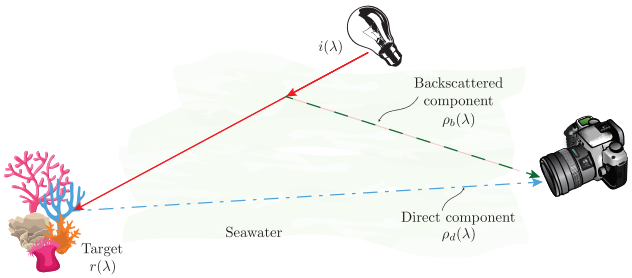

Figure 1: Direct and backscattered components in underwater imaging.

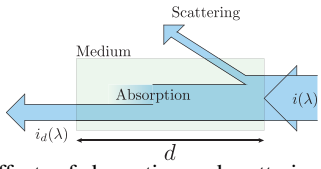

Figure 2: The effects of absorption and scattering on the intensity of light traveling through a medium.

the direct component depends on the light source spectral power distribution $i(\lambda)$, target surface spectral reflectance $r(\lambda)$, and the attenuation of light introduced by the medium $c(\lambda)$. The relationship is governed by the Beer-Lambert attenuation law [4]

$$\rho_d(\lambda) = r(\lambda)i(\lambda)e^{-dc(\lambda)}, \tag{3}$$

where d is the distance light travels through the medium.

Total attenuation coefficient

The total attenuation coefficient $c(\lambda)$ describes how much light at wavelength λ is attenuated as it travels through the medium. Light attenuation depends on how much the medium absorbs light as well as how much light is scattered by. The contributions of these two phenomena, denoted $a(\lambda)$ and $b(\lambda)$ for absorption and scattering respectively, define the total absorption coefficient $c(\lambda)$

$$c(\lambda) = a(\lambda) + b(\lambda). \tag{4}$$

Intuitively, the intensity of a particular ray of light traveling through a medium can be decreased either because photons are absorbed by the medium, or because some of the light starts to propagate in different direction, when it is reflected off small particles suspended in that medium. Along the ray however the net effect of these two distinct phenomena is the same; light intensity is reduced (Fig. 2).

Absorption coefficient

In underwater environments the absorption coefficient is impacted by the optical properties of pure sea water $a_w(\lambda)$ and the absorption properties of three seawater constituent particles: phytoplankton $a_\Phi(\lambda)$, colored dissolved organic matter (CDOM), $a_{CDOM}(\lambda)$, and non-algal particles (NAP), $a_{NAP}(\lambda)$. The total absorption coefficient is given by the sum of absorption properties of the constituents

$$a(\lambda) = a_w(\lambda) + a_\Phi(\lambda) + a_{CDOM}(\lambda) + a_{NAP}(\lambda). \tag{5}$$

Figure 3 shows the shapes of the spectral absorption coefficient of the four constituents. The absorption properties of each of them

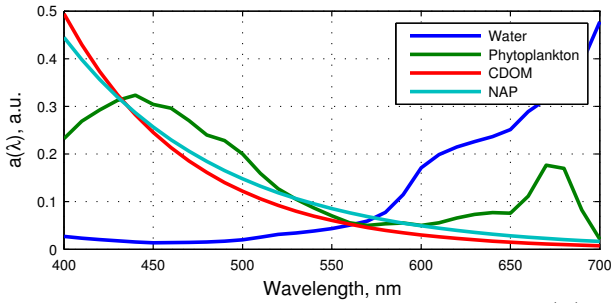

Figure 3: Shapes of the spectral absorption coefficient $a(\alpha)$ for different seawater constituents. Individual components are not shown to scale, y-axis represents arbitrary units.

have been extensively studied. The spectral absorption of pure seawater $a_w(\lambda)$ is fixed and well known [8, 21, 22]. The particular properties of phytoplankton and non-algal particles have both been shown to be related to the concentration of chlorophyll [6]. While the absorption properties of the colored dissolved organic matter, also called yellow matter, are largely independent of the amount of chlorophyll [7, 16].

The CDOM spectral absorption is described well by a decaying exponential [7]

$$a_{CDOM}(\lambda) = a_{CDOM,\lambda_0} e^{-0.014(\lambda-\lambda_0)}, \tag{6}$$

where λ_0, the reference wavelength, is often chosen to be 440nm, and a_{CDOM,λ_0} is the absorption at the reference wavelength. The scale in the exponent was experimentally determined and usually varies between -0.014 and -0.019 [7].

The absorption by non-algal particles (detritus) has a very similar form to that of CDOM [17]

$$a_{NAP}(\lambda) = a_{NAP,\lambda_0} e^{-0.011(\lambda-\lambda_0)}, \tag{7}$$

with values of the scale in the exponent in the range of -0.006 to -0.014 [17]. Furthermore [6] showed that the detritus absorption at $\lambda_0 = 440$ is highly correlated to chlorophyll concentration C

$$a_{NAP,440} = 0.0124 \cdot C^{0.724}. \tag{8}$$

The spectral absorption of phytoplankton depends on its species as well as amout. The amount of phytoplankton is defined by the concentration of chlorphyll, one of its primary components. The spectral shape of the absorption curve is affected by the phytoplankton species. Though many phytoplankton species exist their absorption curves are somewhat similar with peak absorption around 450 and 650nm [11, 18]. These between-species similarities mean that phytoplankton absorption can be compactly represented with low-dimensional linear models

$$c_\Phi(\lambda) = \sum_{i=1}^{z} t_i(\lambda) w_i, \tag{9}$$

where $t_i(\lambda)$ are fixed phytoplankton absorption basis functions and w_i are the absorption basis weights. Furthermore [6] showed that phytoplankton absorption is related to chlorophyl concentration C by

$$c_\Phi(440) = 0.0378 \cdot C^{0.627}. \tag{10}$$

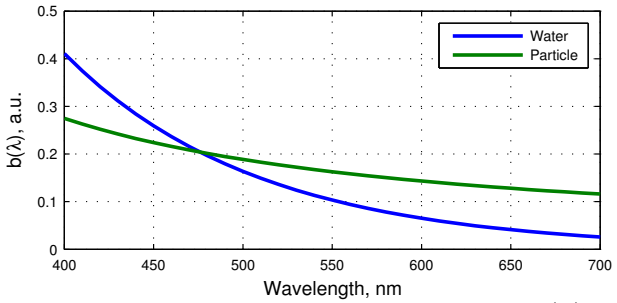

Figure 4: Shapes of the spectral scattering coefficient $b(\alpha)$ for different seawater constituents.

A particular phytoplankton absorption spectrum can be generated by first defining the shape by selecting a particular assignment of weights w. Then the shape can be scaled, to satisfy (10).

Scattering coefficient

The total scattering coefficient $b(\lambda)$ can also be represented as a sum of the scattering coefficients of seawater constituents; pure seawater $b_w(\lambda)$ and particulate matter $b_p(\lambda)$

$$b(\lambda) = b_w(\lambda) + b_p(\lambda). \tag{11}$$

The spectral shapes of this coefficient for the two components are presented in Fig. 4. Just as in the case of absorption, the scattering coefficient of seawater $b_w(\lambda)$ is fixed and known [5]. The scattering coefficient of particulate matter depends on the concentrations of pico-, nano- and microphytoplankton as well as the concentrations of co-varying constituents. The concentrations of different phytoplankton types can be related to the total chlorophyll concentration C [5], and consequently express the total scattering coefficient as a function of C

$$b_p(\lambda) = b^{\star}_{p,1,2,\lambda_0} \left(\frac{\lambda}{\lambda_0}\right)^{-\gamma_{1,2}} \left[C_{1,2}\left(1 - e^{-S_{1,2}C}\right)\right] \tag{12}$$

$$+ b^{\star}_{p,3,\lambda_0} \left(\frac{\lambda}{\lambda_0}\right)^{-\gamma_3} \left[C - C_{1,2}\left(1 - e^{-S_{1,2}C}\right)\right] \tag{13}$$

$$+ b_{k,\lambda_0} \left(\frac{\lambda}{\lambda_0}\right)^{-\gamma_k}. \tag{14}$$

The only free parameter in the above equation is phytoplankton concentration C. The subscript $1,2$ represents the contributions of pico- and nanophytoplankton, while the subscript 3 represents microphytoplankton. Finally, a constant background contribution is given by b_k. All model parameters and the numerical values used are summarized in Table 1

Discrete model

To simplify computation we discretize all spectral quantities to a small number, q of narrow wavelength bands. The continuous wavelength representation of total attenuation

$$k(\lambda) = e^{-da(\lambda)}, \tag{15}$$

is replaced with a vector $k \in \mathbf{R}^q$, whose ith entry represents the total attenuation at wavelength λ_i

$$k_i = e^{-da(\lambda_i)}, \tag{16}$$

Table 1: Particle scattering coefficient model parameters for $\lambda_0 =$ 470nm, data taken from [5].

Parameter	Unit	Value
$C_{1,2}$	mg m^{-3}	0.78
$S_{1,2}$	(mg)$^{-1}$ m^3	1.1449
$b^{\star}_{p,1,2,\lambda_0}$	m^2 mg^{-1}	0.0046
$b^{\star}_{p,3,\lambda_0}$	m^2 (mg)$^{-1}$	0.0005
b_{k,λ_0}	m^{-1}	0.00068
$\gamma_{1,2}$	–	0.7
γ_3	–	-0.2
γ_k	–	1.9

and where d is the distance traveled through the medium. To underline the dependence of the total attenuation k on model parameters $x = (w, C, a_{CDOM,\lambda_0})^T$, the discretized attenuation is denoted $k(x)$.

Parameter estimation

The underwater image formation model can also be used to estimate model parameters from data, i.e. determine phytoplankton absorption spectrum, chlorophyl concentration and amount of color dissolved organic matter, CDOM, from an image of a target with known spectral reflectance. Estimation involves finding a solution to a minimization problem

$$\underset{x,s}{\text{minimize}} \;\; \|M - P^T \mathbf{diag}(i)\mathbf{diag}(k(x))R - s\mathbf{1}^T\|_F^2 \tag{17}$$

$$\text{subject to } C \geq 0,\; a_{CDOM,\lambda_0} \geq 0,\; Tw \geq 0 \tag{18}$$

$$(Tw)_{\lambda_0} = 0.0378 \cdot C^{0.627} \tag{19}$$

$$s \geq 0. \tag{20}$$

The matrix $M \in \mathbf{R}^{m \times n}$ represents pixel intensities of n different surfaces imaged using a camera with m different spectral channels (for color consumer cameras $m = 3$). The columns of $P \in \mathbf{R}^{q \times m}$ are the spectral responsivity functions of the camera, quantized to q spectral bands, the vector $i \in \mathbf{R}^q$ is the spectral power distirbution of the illuminant. The matrix $R \in \mathbf{R}^{q \times n}$ contains n surface spectral reflectanes, and the matrix $T \in \mathbf{R}^{q \times z}$ contains z discrete plankton absorption basis functions. Finally the vector $s \in \mathbf{R}^m$ contains backscattered light estimates for each of the camera channels. These estimates, however are the same for all surfaces.

The minimization problem contains several constraints, all of which follow directly from the physical properties of the estimated quantities. Specifically, phytpolankton spectral absorption TW, chlorophyl cocentration C, CDOM reference absorption a_{CDOM,λ_0} and scattering s are all non-negative quantities. Furthermore the phytoplankton spectral absorption curve needs to be appropriately scaled, so that (10) holds.

The optimization problem (17) is not convex and thus difficult to solve for two reasons. First, the objective function is an l_2 norm of a sum of an exponential function and a constant term; it is therefore non-convex. Second, the equality constraint (19) is not linear. However, all the functions that cause non-convexity of the problem are continuous, smooth and monotonic. Therefore, to solve the problem we use an iterative approach where at iteration t we replace the function $k(x)$ with its first order Taylor series expansion around some estimate x^t. We use a similar approach to

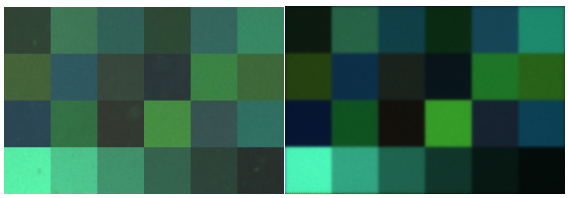

(a) Captured (b) Simulated

Figure 5: Target appearance in clear water conditions (Fanning Island). Images are not gamma encoded.

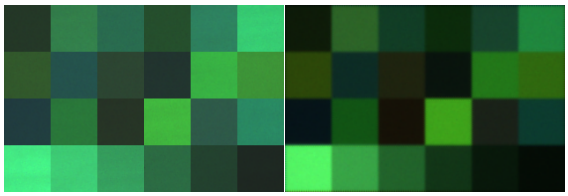

(a) Captured (b) Simulated

Figure 6: Target appearance in murky water conditions (Monterey Bay, CA). Images are not gamma encoded.

replace the non-linear equality constraint (19) with its first order Taylor series expansion around C^t. The minimization provides parameter estimates that are used at center points for Taylor series expansion at the next iteration. And the process is repeated until no decrease in the objective is observed.

Experiments

We implemented the underwater image formation model in Matlab and used the Image Systems Engineering Toolbox to simulate camera acquisition of a Macbeth test chart placed underwater [10]. We used a model of a typical, consumer camera with a Bayer RGB color filter array and a near infrared (NIR) filter. Convex optimization problems were solved with `cvx` optimization toolbox [12]. We simulated different water types by varying the concentrations of chlorophyll C, the absorption of color dissolved organic matter CDOM, a_{CDOM,λ_0}. We chose $\lambda_0 = 440$nm as the reference wavelength for CDOM absorption estimates and we used phytoplankton basis functions derived from data from [11]. This particular data set proved to be largely one-dimensional, and hence we chose a single basis function. Consequently the shape of phytoplankton absorption was fixed, and only the scale could vary, even though the proposed algorithm can handle cases where phytoplankton absorption shape varies. Finally, we generated tests scenes at different depths and camera to target distances.

Appearance simulation

We evaluate our model using qualitative comparison between simulated target images and the images of a Macbeth chart submerged in different locations. Figure 5 shows target appearance in clear waters of the Pacific Ocean in the proximity of Fanning Island. The blueish tint of the simulated test target was achieved by setting a low chlorophyll concentration $C = 1\text{mg m}^{-1}$ and low CDOM absorption $a_{CDOM,440} = 0.05\text{m}^{-1}$. Figure 6 presents a similar comparison for murky waters of the Monterey Bay, CA. To obtain a much stronger greenish tint of the target the chorophyll concentration was increased to $C = 5\text{mg m}^{-1}$ and CDOM absorption was set to $a_{CDOM,440} = 0.1\text{m}^{-1}$.

Figure 7 further explore the changes in the appearance of the test target when different model parameters are selected. Specifically color appearance changes are much more pronounced with increasing target depth (Fig. 7, top row). As light travels deeper underwater, it is attenuated more and more strongly and the colors become less and less pronounced. Changes in the camera to target distance (Fig. 7, bottom row) have a much smaller effect on the overall color appearance.

Figure 8 shows appearance changes as the function of chlorophyll concentration. The concentration was adjusted between $C = 0.01\text{mg m}^{-1}$ (open ocean waters) and $C = 100\text{mg m}^{-1}$ (eutropic estuaries or lakes) [16]. As expected the overall hue changes from blueish, characteristic of pure water absorption, to greenish, where absorption is dominated by phytoplankton.

Parameter estimation

The estimation algorithm finds such assignment of the model parameters $x = (w, C, a_{CDOM,\lambda_0})^T$ so that the resulting light attenuation $k(x)$ produces the best fit between the image formation model and the measured or simulated data M. Figure 9 presents a sample attenuation estimate $k(x)$ (blue) as well as the ground truth data (green) for a particular set of medium properties and scene geometry.

The high quality of the estimate does not depend on the specific medium characteristics. Figure 10 presents the relative root-mean-squared error (RRMSE) defined as

$$\text{RRMSE} = \frac{\|\hat{y} - y\|}{\sqrt{q}\|y\|}, \tag{21}$$

where $y, \hat{y} \in \mathbf{R}^q$ represent the true and estimated quantity respectively. The RRMSE values are computed for different depths and camera to scene distances and averaged across different chlorophyll concentrations and CDOM absorption values. Note that this relative error remains small, about 2%, but increases slightly with larger depths and target distances.

The wavelength dependence of the spectral attenuation $k(\lambda)$ is the reason why underwater imaging introduces color changes. As the light travels deeper into the medium, its spectral composition, and thus colors, are affected. The information about the shape of spectral absorption curve is invaluable if one is interested in color correction. Figure 11, left, presents the appearance of the underwater target used to derive the attenuation curve from Fig. 9. This attenuation curve was then used to estimate the illuminant and use this estimate in the diagonal von Kries model mapping [23] to perform illuminant correction. After the correction (Fig 11, right), the surface appearance of the Macbeth chart has been recovered.

Given that the algorithm can predict medium attenuation with high accuracy it is necessary to investigate how the model parameters given by the estimation algorithm correlate with the ground truth values. It may be possible that different numerical values of model parameters x can produce the same spectral attenuation curves, making the estimation problem ill-posed.

Figure 12 presents a comparison between ground truth and phytoplankton concentration C estimates in different conditions and for different scene geometries. Pearson's correlation coefficient between the true and estimated quantities is high; 0.7 or more. We noticed that concentration estimates tend to be less accurate with increasing depth and for water types with low absorption of colored dissolved organic matter, CDOM.

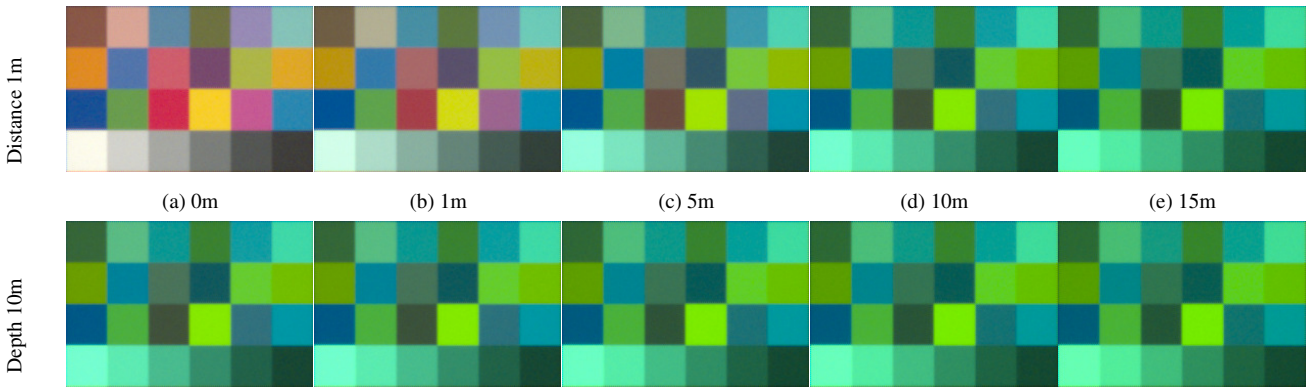

(a) 0m (b) 1m (c) 5m (d) 10m (e) 15m

(f) 1m (g) 2m (h) 5m (i) 7m (j) 10m

Figure 7: Macbeth test target appearance for different scene geometries: targed distance and depth, $a_{CDOM,440} = 0.1\text{m}^{-1}$, $C = 1\text{mg m}^{-3}$.

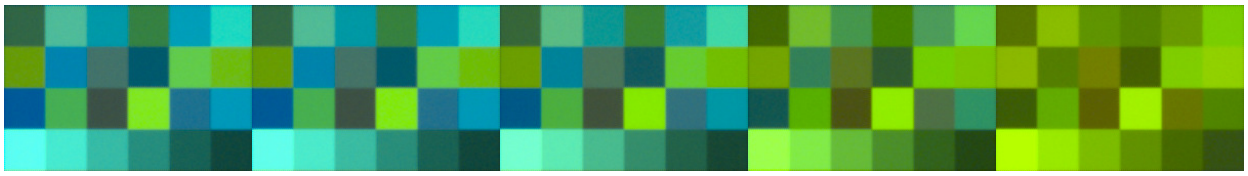

(a) 0.01mg m^{-3} (b) 0.1mg m^{-3} (c) 1mg m^{-3} (d) 10mg m^{-3} (e) 100mg m^{-3}

Figure 8: Macbeth test target appearance for different chlorophyll concentrations. The target is submerged to 10m and is 1m away from the camera, $a_{CDOM,440} = 0.1\text{m}^{-1}$.

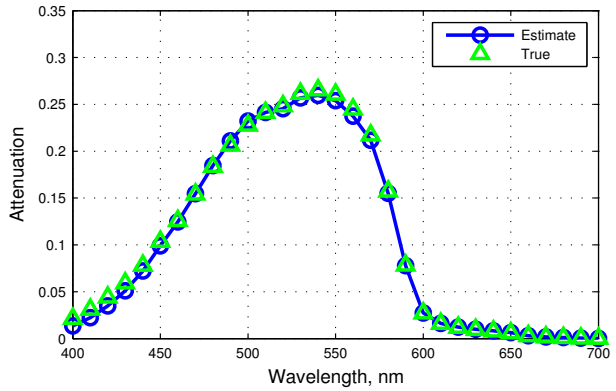

Figure 9: Light attenuation estimation example, depth 10m, distance 5m, $C = 1\text{mg m}^{-3}$ and $a_{CDOM,440} = 0.1\text{m}^{-1}$.

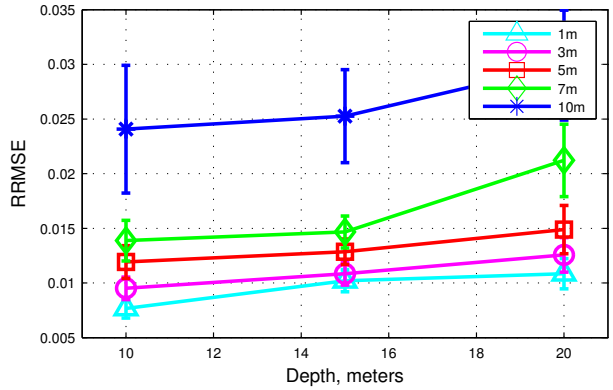

Figure 10: Erros in light attenuation estimation. Each point represents the average RMSE and the corresponding standard error across different phytoplankton concentrations C and CDOM absoprtions $a_{CDOM,440}$.

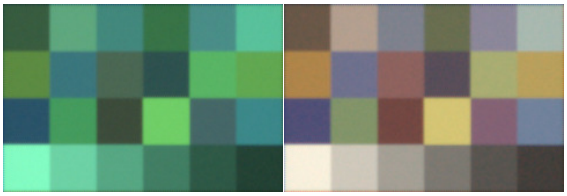

(a) (b)

Figure 11: Color correction of underwater image. The original image (a) was used to estimate the absorption. The estimated absorption provided the von Kires model coefficients for illuminant correction (b).

Similar analysis, presenting the correlation between the true and estimated colored dissolved organic matter (CDOM) absorption

Conclusions

References

[1] Julia Åhlén, David Sundgren, and Ewert Bengtsson. Application of underwater hyperspectral data for color correction purposes. *Pattern Recognition and Image Analysis*, 17(1):170–173, 2007.

[2] Henryk Blasinski, John Breneman, and Joyce Farrell. A model for estimating spectral properties of water from rgb images. In *IEEE International Conference on Image Processing ICIP*, pages 610–614, Oct 2014.

[3] Matthieu Boffety, Frédéric Galland, and Anne-Gaëlle Allais. Color image simulation for underwater optics. *Applied optics*, 51(23):5633–5642, 2012.

[4] John Breneman, Henryk Blasinski, and Joyce Farrell. The color of water: using underwater photography to assess water quality. In *IS&T/SPIE Electronic Imaging*, pages 90230R–90230R. International Society for Optics and Photonics, 2014.

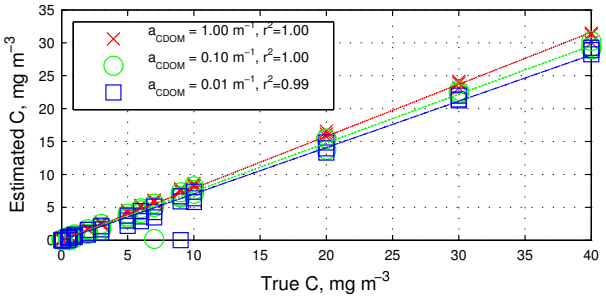

(a)

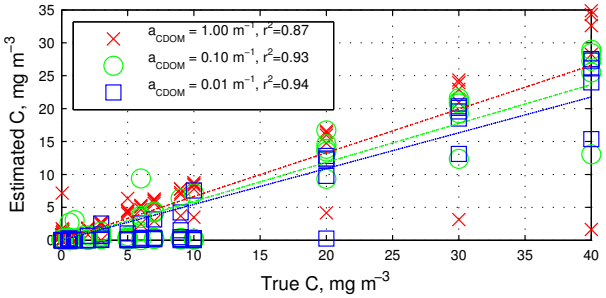

(b)

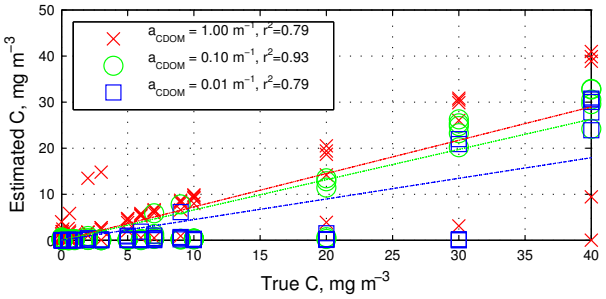

(c)

Figure 12: Chlorophyll concentration estimation accuracy for a fixed scene to target distance of 1m, different depths: (a) 5m, (b) 10m, (c) 20m and different values of $a_{CDOM,440}$. In all cases the Pearson's correlation coefficient r^2 is high, though it decreases with an increase in depth and lower CDOM absorption values.

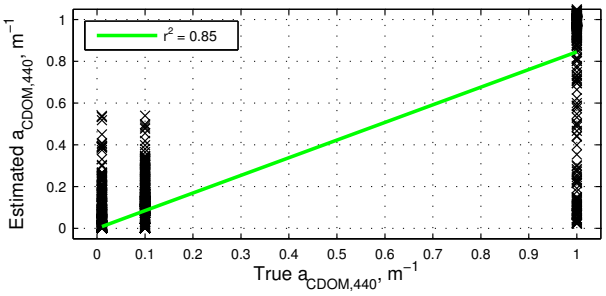

Figure 13: Colored dissolved organic matter (CDOM) absorption at 440nm. Each sample point represents the $a_{CDOM,440}$ estimate for different scene to target distances, depths and chlorophyll concentrations.

[5] Robert Brewin, Giorgio DallOlmo, Shubha Sathyendranath, and Nick Hardman-Mountford. Particle backscattering as a function of chlorophyll and phytoplankton size structure in the open-ocean. *Optics express*, 20(16):17632–17652, 2012.

[6] Annick Bricaud, Andre Morel, Marcel Babin, Karima Allali, and Herve Claustre. Variations of light absorption by suspended particles with chlorophyll a concentration in oceanic (case 1) waters: Analysis and implications for bio-optical models. *Journal of Geophysical Research: Oceans*, 103(C13):31033–31044, 1998.

[7] Annick Bricaud, Andre Morel, and Louis Prieur. Absorption by dissolved organic matter of the sea (yellow substance) in the UV and visible domains. *Limnology Oceanogr*, 26(1):43–53, 1981.

[8] Hendrik Buiteveld, JHM Hakvoort, and M Donze. Optical properties of pure water. In *Ocean Optics XII*, pages 174–183. International Society for Optics and Photonics, 1994.

[9] John Y Chiang and Ying-Ching Chen. Underwater image enhancement by wavelength compensation and dehazing. *IEEE Transactions on Image Processing*, 21(4):1756–1769, 2012.

[10] J. E. Farrell, P. B. Catrysse, and B. A. Wandell. Digital camera simulation. *Applied Optics*, 51:A80–A90, 2012.

[11] Tetsuichi Fujiki and Satoru Taguchi. Variability in chlorophyll-a specific absorption coefficient in marine phytoplankton as a function of cell size and irradiance. *Journal of Plankton Research*, 24(9):859–874, 2002.

[12] Michael Grant and Stephen Boyd. CVX: Matlab software for disciplined convex programming, version 2.1. `http://cvxr.com/cvx`, March 2014.

[13] Jules Jaffe. Computer modeling and the design of optimal underwater imaging systems. *IEEE Journal of Oceanic Engineering*, 15(2):101–111, 1990.

[14] ZhongPing Lee, Kendall L. Carder, and Robert A. Arnone. Deriving inherent optical properties from water color: a multiband quasi-analytical algorithm for optically deep waters. *Applied Optics*, 41(27):5755–5772, Sep 2002.

[15] BL McGlamery. A computer model for underwater camera systems. In *Ocean Optics VI*, pages 221–231. International Society for Optics and Photonics, 1980.

[16] Curtis Mobley. *Light and water: Radiative transfer in natural waters*. Academic Press, 1994.

[17] Collin Roesler, Mary Perry, and Kendall Carder. Modeling in situ phytoplankton absorption from total absorption spectra in productive inland marine waters. *Limnology and Oceanography*, 34(8):1510–1523, 1989.

[18] Shubha Sathyendranath, Luigi Lazzara, and Louis Prieur. Variations in the spectral values of specific absorption of phytoplankton. *Limnology and Oceanography*, 32(2):403–415, 1987.

[19] Raimondo Schettini and Silvia Corchs. Underwater image processing: state of the art of restoration and image enhancement methods. *EURASIP Journal on Advances in Signal Processing*, 2010:14, 2010.

[20] Anne Sedlazeck and Reinhard Koch. Simulating Deep Sea Underwater Images Using Physical Models for Light Attenuation, Scattering, and Refraction. In Peter Eisert, Joachim Hornegger, and Konrad Polthier, editors, *Vision, Modeling, and Visualization*. The Eurographics Association, 2011.

[21] Raymond Smith and Karen Baker. Optical properties of the clearest natural waters (200–800nm). *Applied optics*, 20(2):177–184, 1981.

[22] Seraphin Sullivan. Experimental study of the absorption in distilled water, artificial sea water, and heavy water in the visible region of

the spectrum. *Journal of the Optical Society of America*, 53(8):962–967, 1963.

[23] Johann von Kries. Die gesichtsempfindungen. *Handbuch der physiologie des menschen*, 3:109–282, 1905.

[24] Brian Wandell. *Foundations of vision.* Sinauer Associates, 1995.

[25] Xinwei Zhao, Tao Jin, and Song Qu. Deriving inherent optical properties from background color and underwater image enhancement. *Ocean Engineering*, 94:163–172, 2015.

Author Biography

Henryk Blasinski received the M.S. degree (Hons.) in telecommunications and computer science from the Lodz University of Technology, Lodz, Poland, and the Diplome d'Ingeneiur degree from the Institut Superieur dElectronique de Paris, France, in 2008 and 2009, respectively. He was a Fulbright Scholar with the Department of Electrical and Computer Engineering, University of Rochester, Rochester, NY, from 2010 to 2011. At present he is pursuing a Ph.D. degree at the Department of Electrical Engineering, Stanford University, CA. Henryk's research interests include image processing, human and computer vision and machine learning.

Joyce Farrell is the Executive Director of the Stanford Center for Image Systems Engineering and a senior research associate in the Department of Electrical Engineering at Stanford University. She has a doctorate degree from Stanford University and more than 20 years of research and professional experience working at a variety of companies and institutions, including the NASA Ames Research Center, New York University, the Xerox Palo Alto Research Center, Hewlett Packard Laboratories and Shutterfly.